Advances in Geo-Energy Research

Vol. 4, No. 4, p. 419-434, 2020

Original article

Pore-scale numerical simulation of supercritical CO_2 migration in porous and fractured media saturated with water

Hejuan Liu[1,2], Zhengwen Zhu[3], Were Patrick[4], Jianfeng Liu[5,6]*, Hongwu Lei[1,2], Liwei Zhang[1,2]

[1] *State Key Laboratory of Geomechanics and Geotechnical Engineering, Institute of Rock and Soil Mechanics, Chinese Academy of Sciences, Wuhan 430071, P. R. China*

[2] *University of Chinese Academy of Sciences, Beijing 100049, P. R. China*

[3] *Institute of Architectural Engineering, Sichuan Institute of Industrial Technology, Deyang 618209, P. R. China*

[4] *Energie-Forschungszentrum Niedersachsen, Clausthal University of Technology, Goslar 38640, Germany*

[5] *State Key Laboratory of Hydraulic and Mountain River Engineering, Sichuan University, Chengdu 610065, P. R. China*

[6] *Key Laboratory of Deep Earth Science and Engineering, Ministry of Education, Sichuan University, Chengdu 610065, P. R. China*

Keywords:
Two-phase flow
phase field method
displacement
preferential flow
fractured media

Cited as:
Liu, H., Zhu, Z., Patrick, W., Liu, J., Lei, H., Zhang, L. Pore-scale numerical simulation of supercritical CO_2 migration in porous and fractured media saturated with water. *Advances in Geo-Energy Research*, 2020, 4(4): 419-434, doi: 10.46690/ager.2020.04.07.

Abstract:
A thorough understanding of the microscopic flow process in porous and fractured media is significant for oil and gas development, geothermal energy extraction and subsurface CO_2 storage etc. In CO_2 geological sequestration, the CO_2 is often injected at the supercritical state ($scCO_2$), which will displace the connate fluids in the pore spaces during the drainage process. However, when CO_2 injection stops, the connate brine or water flows back to displace the $scCO_2$. Therefore, the configuration of migration paths in a specific reservoir plays a significant role in affecting the connectivity and storage efficiency of $scCO_2$. In this paper, the two-phase ($scCO_2$ and water) boundary has been defined using the phase field method, and the COMSOL Multiphysics simulator is applied to study the migration of $scCO_2$ in porous/fractured media at the pore scale. The geological conditions of Shiqianfeng formation in the CO_2 capture and storage pilot site of the Ordos Basin in China is selected as the engineering background. Before using the actual microscopic geometry based on thin-section of Shiqianfeng sandstone, we get the general understanding on $scCO_2$ migration in fractured porous media that has the highly simplified configuration with circular particles, considering the impacts of wettability, geometry of formation mineral grains, interfacial tension, injection rates, and fracture geometry. Results show that the CO_2 preferential flow occurs at locations with high CO_2 flow rates and high CO_2 pore pressure. The preferential flow of $scCO_2$ occurs adjacent to the wall of grains while minimal or little flow takes place through the interior between the grains, considering the grains with irregular shapes. The interfacial tension of porous media plays a significant role in controlling the spatial distribution of the $scCO_2$. A much lower interfacial tension results in a much thinner $scCO_2$ flow band with a much higher saturation. The geometry of fractures in porous media increases the complexity of the $scCO_2$ flow paths at the pore scale.

1. Introduction

The injection of CO_2 into the subsurface saline formations at a depth more than 800 m has proven to be technically feasible in many countries, including the USA, Netherlands, Canada, Australia, China etc (Liu et al., 2017). The injected CO_2 can also be used to chemically reactive with the low permeability reservoir in order to increase the hydraulic conductivity (Kizaki et al., 2012), and to enhance the recovery of oil, natural gas, shale gas and geothermal energy (Liu et al., 2015; Singh, 2018; Zhou et al., 2019). The geological storage of CO_2 is mainly facilitated by means of several mechanisms, including structural or stratigraphic trapping, residual or capillary trapping, solubility trapping and mineral trapping (Metz et al., 2005; Parry et al., 2007; Benson and

Yandy Scientific Press

*Corresponding author.
E-mail address: hjliu@whrsm.ac.cn (H. Liu); zhuzw0104@163.com (Z. Zhu); patrickwere@ymail.com (W. Patrick); liujf@scu.edu.cn (J. Liu); hwlei@whrsm.ac.cn (H. Lei); lwzhang@whrsm.ac.cn (L. Zhang).

Received September 23, 2020; revised October 10, 2020; accepted October 10, 2020; available online October 17, 2020.

Cole, 2008; Chaudhary et al., 2013). Among them, residual or capillary trapping is the most effective mechanism for the long-term geological storage of CO_2 in subsurface (Benson and Cole, 2008; Suekane et al., 2011; Andrew et al., 2015). However, residual gas trapping mechanism is strongly formation-specific, whereby the residual CO_2 saturation may be as high as 15%-25% in a typical storage formation during post-injection migration (Holtz, 2002). In a few exceptional cases, however, residual CO_2 trapping mechanism in a suitable formation can enable attainment of storage as high as 90% of the total injected volume of CO_2 (Chaudhary et al., 2013).

The supercritical CO_2 flow in the subsurface involves multi-scales (ranging from mm to km), multiple phases (including supercritical CO_2 phase, liquid phase and solid phase), coupling of different physical and chemical fields (thermal-hydro-mechanical-chemical), and different kinds of reservoirs, e.g., saline formations, unmineable coal seam, depleted oil or gas reservoirs and rock salt caverns. In CO_2 geological sequestration, the injected CO_2 can displace the connate fluids stored in the pore spaces during the supercritical CO_2 ($scCO_2$) flooding, also called the drainage process. The imbibition occurs when the brine or water flows back to the pores and the $scCO_2$ is displaced after the CO_2 injection stops (Hu et al., 2017). Migration path of $scCO_2$ is a significant factor in controlling the chemical interactions and other properties in the reservoir (Liu et al., 2015), thus affecting the efficiency of CO_2 injectivity and storage. The $scCO_2$ flow or trapping in the microscopic porous or fractured media exhibits a wide range of similarities with that of the microscopic water displacing residual oil. The $scCO_2$ flow paths are affected by wettability (Chaudhary et al., 2013; Holtzman and Segre, 2015; Trojer et al., 2015; Hu et al., 2017), size, shape and number of solid particles (Sun et al., 2017).

The $scCO_2$ migration and storage in the natural sandstone or glass beads at the core scale, either homogeneous or heterogeneous, during the drainage process of the core flooding experiments are widely studied using many physical experimental tools: (1) the traditional optical technique by examining thin-sections in transmitted and reflected light or microscopic simulation model (e.g., a pore-scale network model, rock etching model) (Mattax, 1961; Jamaloei et al., 2010; Al-Shalabi and Ghosh, 2016); (2) scanning electron microscopy to observe the wettability of $scCO_2$ film on the surface of mineral grains, while considering the impacts of composition, size and distribution on micro-scale fluid flow (Combes et al., 1998; Kareem, 2015); (3) confocal laser scanning microscopy; (4) the greatly developed computed tomography (CT) technology, which can realize the three-dimensional (3D) visualization with a high resolution (several μm) and has already been widely used in investigating the distribution of residual oil (Turner et al., 2004; Youssef et al., 2010; Iglauer et al., 2012) or $scCO_2$ (Perrin and Benson, 2010; Krevor et al., 2012; Wang et al., 2013; Wei et al., 2014; Zhang et al., 2014; Miao et al., 2019; Xu et al., 2020); and (5) nuclear magnetic resonance imaging that is also widely used in studying fluid distribution in porous or fractured media at mm or μm resolution (Baldwin and Yamanashi, 1989; Suekane et al., 2009; Song et al., 2012; Yu et al., 2014; Prather, 2015).

Numerical simulation is a powerful tool for investigating multiphase fluid flow in porous/fractured media at the pore-scale (Xu et al., 2011; Shakibaeinia and Jin, 2012; Zhu et al., 2016). Generally, different numerical methods based on a variety of algorithms are used, including: (1) grid-based methods (e.g., finite element method, finite difference method and finite volume method); (2) mesh free methods (e.g., smoothed particle hydrodynamics (SPH), lattice boltzmann method (LBM) (Ramstad et al., 2019), molecular dynamics method; dissipative particle dynamics; moving particle semi-implicit methods, etc); and (3) pore network modelling method (e.g., quasi static and dynamic pore network methods). Definition of the phase boundary in the grid-based methods is achieved using one of the following methods: (1) the moving mesh method; (2) the surface tracking method; and (3) the volume tracking method (Raeini et al., 2012). At the pore scale, the phase boundary in the grid-based methods can also be defined through the volume-of-fluid method, which is applied in the ANSYS and Fluent (Yan and Sun, 2016). Besides, the level set method is also used in tracking the movement of phase boundary (Osher and Sethian, 1988). Based on Ginzburg-Landau theory, the phase field method (Antannovskii, 1995; Jacqmin, 1999), which is one of the diffuse interface methods that was presented by van der Waals (1894), uses the phase-field variable to track the phase boundary (Ginzburg and Landau, 1950; Cahn and Hilliard, 1958; Chen, 2002). The fourth order partial differential Cahn-Hilliard function is used to control the evolution of phase-field variable (Bogdanov et al., 2011). In the mesh free numerical methods, the SPH and LBM are widely considered in microscopic fluid flow. The pore-scale multiphase flow behavior is complex, which is highly dependent on influences of roughness (Lenormand and Zarcone, 1984), disorder distribution of grains (Holtzman 2016), wettability (Herring et al., 2016; Hu et al., 2017) and contact angle of porous media, etc (Al-Futaisi and Patzek, 2003).

In general, numerical simulation results are highly dependent on the microscopic structures of the rock, which show the strong heterogeneity at the pore-scale. For the geometry of the micro-models used in CO_2 flooding experiments, most authors applied a homogeneous model that consists of round glass beads (Chaudhary et al., 2013) or etched on the silica plates with hydrofluoric acid (Hu et al., 2017), in which the heterogeneity of pore structure is also considered. The construction of a 3D porous model mainly involves X-ray CT, the focused ion beam-scanned electronic microscopy, sequential indicator simulation, multiple point statistics, pore network model and nuclear magnetic resonance imaging (Minto, 2014). It is worth highlighting that the construction of two-dimensional (2D) micro-structure of porous media based on the rock thin-section method is still widely engaged by many researchers because the X-ray CT technique is very expensive to be widely applied. In addition, image processing techniques, such as the Gaussian field method and the simulated-annealing approach, are often used (Joshi, 1974; Yeong and Torquato, 1998).

The objective of this paper is to study the $scCO_2$ displacement in heterogeneous porous and fractured media at the pore scale. The phase-field theory, including the physical equations

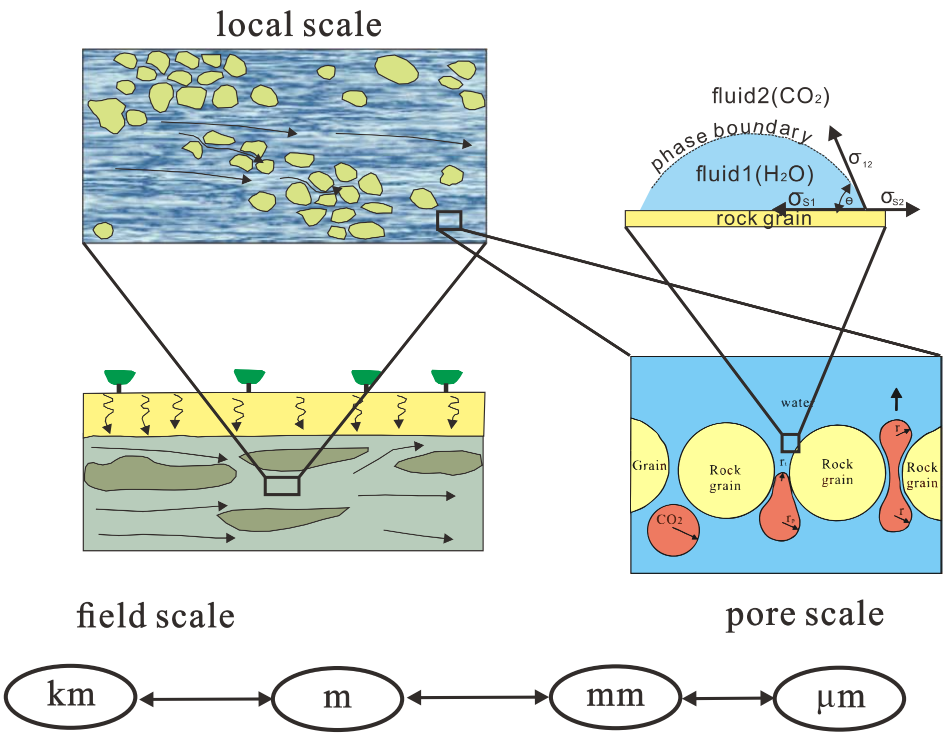

Fig. 1. Illustration of CO_2 flow in porous media at different scales from km to μm (modified from Kobus and de Haar, 1995; IEA, 2011).

of viscous fingering and fluid flow in porous media at the pore scale is studied. Section 3 presents the numerical model and parameters input in the COMSOL Multiphysics simulator, considering the impacts of packing spheres styles, fracture geometry (e.g., single, Y-shape, T-shape and random fractures) and the injection rates at the inlet.

2. Mathematical model

2.1 Viscous fingering

The two-phase fluid (i.e., $scCO_2$ and water) interactively flow in porous media at different scales ranging from field-scale in km to pore-scale in μm (see Fig. 1). As $scCO_2$ migrates in porous media, the migration paths and phase boundary are highly affected by the interfacial tension between two-phases and the contact angles at the surfaces of rock grains:

$$\cos\theta = \frac{\sigma_{s2} - \sigma_{s1}}{\sigma_{12}} \tag{1}$$

where θ is the contact angle (°), and σ_{12}, σ_{s1} and σ_{s2} are the interfacial tension (Pa) between fluid1 and fluid2, fluid1 and the rock grain, fluid2 and the rock grain, respectively.

Two dimensionless factors, i.e., capillary number (Ca) and viscosity ratio (M), are used to relate various forces during the $scCO_2$ displacement in the two-phase flow:

$$Ca = \frac{\mu_2 V_2}{\sigma_{12}\cos\theta} \tag{2}$$

$$M = \frac{\mu_2}{\mu_1} \tag{3}$$

where μ_1 and μ_2 are the viscosities of the displacing fluid (i.e., $scCO_2$) and the displaced fluid (i.e., connate water), respectively (Pa·s); and V_2 is the bulk velocity of the displacing fluid (m^3/s); σ_{12} is the interfacial tension between $scCO_2$ and connate water (Pa).

Note that some $scCO_2$ may be trapped in the pore spaces by capillary forces after CO_2 injection stops (Obdam et al., 2003; Kumar et al., 2005). This is highly controlled by the interfacial tension (σ_{12}) between $scCO_2$ and water. In fact, the interfacial tension not only affects $scCO_2$ flow during the drainage process, but also controls the capillary-sealing efficiency during the imbibition process. When the migration pressure (P_d) of $scCO_2$ is less than the capillary pressure difference (ΔP_c), $scCO_2$ will be trapped in pores as the residual gas (Fig. 1):

$$P_d < \triangle P_c = 2\sigma_{12}\left(\frac{1}{r_t} - \frac{1}{r_p}\right) \tag{4}$$

$$P_c = P_{CO_2} - P_W = \frac{2\sigma_{12}\cos\theta}{r} \tag{5}$$

where r_t, r_p and r are the radius of the pore throat, pore and capillary tube (m), respectively.

2.2 Phase boundary based on the phase field theory

Based on the mass conservation equation, the continuity equation of fluid flow in porous media can be expressed as:

$$\rho \bigtriangledown \cdot \mathbf{u} = 0 \tag{6}$$

where $\mathbf{u}$ is the fluid flow rate in porous media (m/s); ρ is the fluid density (kg/m^3).

The modified Navier-Stokes equation is used to describe the two-phase fluid flow in porous media and fractures at the pore-scale:

$$\rho\frac{\partial \mathbf{u}}{\partial t}+\rho(\mathbf{u}\cdot\nabla)\mathbf{u}=-\nabla p\mathbf{I}+\nabla\cdot\left[\mu\left(\nabla\mathbf{u}+(\nabla\mathbf{u})^T\right)\right]+G\nabla\kappa \quad (7)$$

where p is the pore pressure (Pa); $G=\eta\left[-\nabla^2\kappa+\left(\kappa^3-\kappa\right)/\varphi^2\right]$ is the chemical potential (J/m), representing the variation rate of free energy at the interface of two-phases; ρ is the density of the mixture (kg/m^3): $\rho=\rho_w(1+\kappa)/2+\rho_{CO_2}(1-\kappa)/2$, κ is the phase-field variable, ρ_w and ρ_{CO_2} are the water and CO_2 densities, respectively.

The Cahn-Hilliard phase-field method coupled with the above Navier-Stokes and continuity equations is applied to solve the interfacial problems of spontaneous drainage in the two-phase system (Yue et al., 2004, 2006; Rokhforouz and Akhlaghi Amiri, 2017):

$$\frac{\partial\kappa}{\partial t}+\mathbf{u}\cdot\nabla\kappa=\gamma\eta\nabla^2\left[-\nabla^2\kappa+\frac{\kappa\left(\kappa^2-1\right)}{\varphi^2}\right] \quad (8)$$

In the case of the two-phase flow in porous media at the pore-scale, $-1<\kappa<1$ represents the phase interface, $\kappa=1$ represents the pure continuous phase (water) and $\kappa=-1$ represents the pure disperse phase (i.e., $scCO_2$). The phase-field order parameter (κ) is defined such that the relative concentration of the two components (CO_2 and water) are (1+κ)/2 and (1-κ)/2. φ is the capillary width, equivalent to the thickness of the diffuse interface between the two-phases (m). If φ is too large, the diffuse interface will be blurred. But if it is too small, the calculation rate is very slow. Generally, φ can be equal to or more than half the mesh size in order to smoothly describe the phase function κ; γ is the mobility (m^3·s/kg), $\gamma=\chi\varphi^2$ and χ is the mobility tuning parameter (m·s/kg) expressed in Bai et al. (2017); η is the mixing energy density stored in the thin interface region of the two-phases (N); γ determines the relaxation time of the interface and is defined empirically; t is time (s).

The mobility of $scCO_2$ in porous media can be described as:

$$\gamma=\frac{k_{CO_2}}{\mu_e} \quad (9)$$

where k_{CO_2} is the effective permeability of $scCO_2$ flowing through porous medium (m^2); μ_e is the equivalent viscosity of the binary fluids and $\mu_e=\sqrt{\mu_w\mu_{CO_2}}$, here μ_w and μ_{CO_2} represent the viscosity of water and $scCO_2$, respectively.

In a specific physical system, the empirical expression of mobility γ can be written as (Bai et al., 2017):

$$\gamma=\frac{(C_nL)^2}{16\mu_e} \quad (10)$$

where C_n is the critical Cahn number for the convergence of shape interface limit (-); L is the characteristic length of the specific geometry (m).

The interfacial tension σ can be empirically expressed as a function of the capillary width and the mixing energy density (Yue et al., 2004):

$$\sigma=\frac{2\sqrt{2}}{3}\frac{\eta}{\varphi} \quad (11)$$

The volume fraction of CO_2 and water can be calculated from the following equation defined in Bai et al. (2017):

$$\begin{aligned}V_{fCO_2}&=\frac{1-\kappa}{2}\\ V_{fw}&=\frac{1+\kappa}{2}\end{aligned} \quad (12)$$

The fluid density and viscosity at the interface can be defined as (Bai et al., 2017):

$$\begin{aligned}\rho&=\rho_w+(\rho_{CO_2}-\rho_w)V_{fCO_2}\\ \mu&=\mu_w+(\mu_{CO_2}-\mu_w)V_{fCO_2}\end{aligned} \quad (13)$$

where ρ_w and ρ_{CO_2}represent the density of water and $scCO_2$, respectively.

3. Numerical model

3.1 Geometry setup

It is no doubt that the $scCO_2$ migration in fractured porous media is very complicated due to the strong heterogeneity (mineral composition, mineral configuration, pore and pore throat distribution, etc.) in natural geological condition. From this point of view, it is impossible to grasp the accurate description of $scCO_2$ because of the high simplification of pore structure more or less. In order to get a general understanding on $scCO_2$ displacement in porous and fractured media, the simulation in this paper starts from a highly simplified configuration of circular particles. The 2D micro-structure model, with the length of 20 mm and the width of 15 mm, is randomly generated using four groups of circular grains, each with a different radius (i.e., 0.7, 0.5, 0.4 and 0.3 mm) representing the heterogeneity of mineral size, see Fig. 2. The triangular meshes are applied in the discretization of the 2D geometry.

3.2 Input parameters in the baseline numerical model

The input parameters in the baseline numerical model, including density and viscosity, are based on the CO_2 sequestration site conditions located in the Ordos Basin, China, see details in our previous studies (Liu et al., 2014a, 2014b). The porous media is assumed to be initially saturated with water, which has the density and viscosity of 1000 kg/m^3 and 1 mPa·s, respectively. The brine-$scCO_2$ interfacial tension is highly dependent on the salt concentration, temperature and pressure. In this paper, the brine-$scCO_2$ interfacial tension at the temperature and pore pressure of 75 °C and 18 MPa is set to be 27 mN/m, based on experimental measurements of Chalbaud et al. (2006). The contact angle in porous medium is assumed to be 60° representing water wetting sandstone of the reservoir in the Ordos Basin. The density and viscosity of $scCO_2$ at the fixed temperature (i.e., 75 °C) and pressure (i.e.,

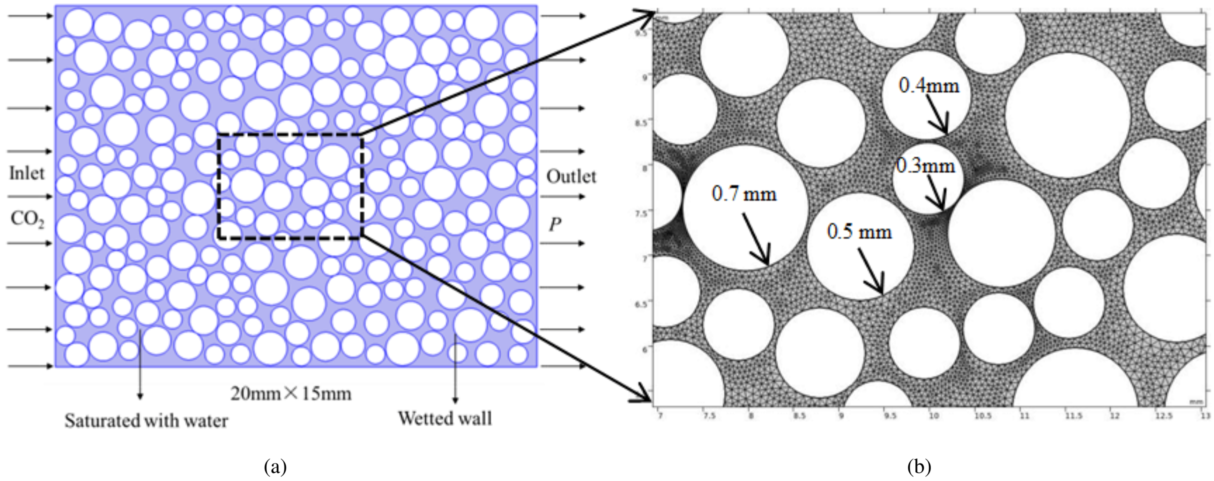

Fig. 2. (a) The two-dimensional geometry of simplified porous media with boundary conditions, (b) discretization of meshes.

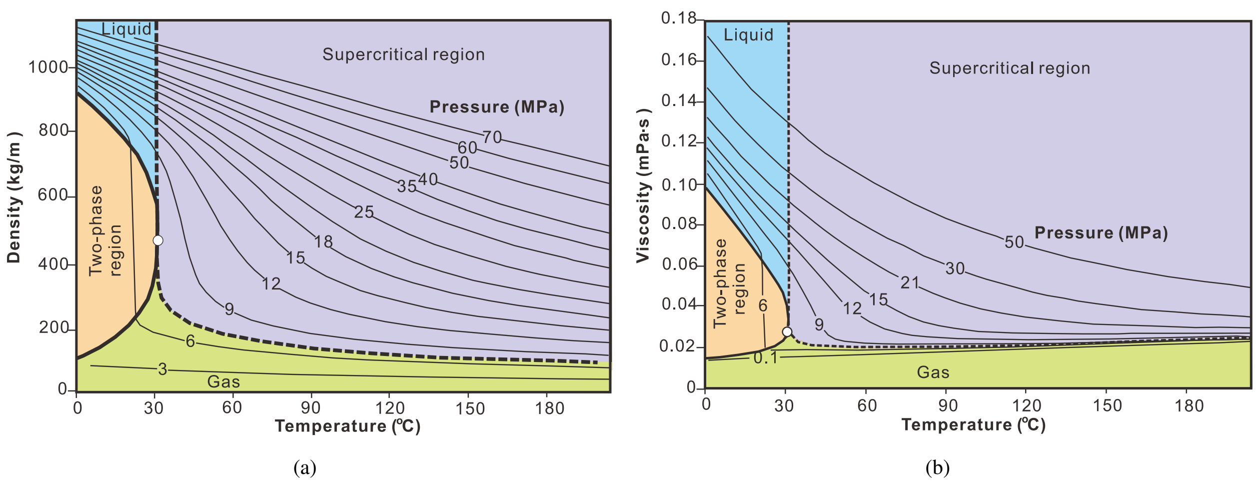

Fig. 3. The density (a) and viscosity (b) of CO_2 under different temperature and pressure conditions (modified from Bachu, 2003).

Table 1. Densities, viscosities and interfacial tension of water and $scCO_2$ at 75°C and 18 MPa used in the baseline simulation.

	Water	$scCO_2$
Density (kg/m^3)	1,000	600
Viscosity (mPa·s)	1	0.05
Contact angle (°)	60	
Interfacial tension (mN/m)	0.05	

18 MPa), are set to be 600 kg/m^3 and 0.05 mPa·s based on the calculations from the phase diagram of CO_2 in Fig. 3, detailed parameters can be seen in Table 1.

In this study, CO_2 is injected from the left boundary at a rate of 10 mm/s. Based on the phase-field theory, only two additional parameters, namely the interfacial thickness φ and the mobility tuning parameter χ, are adjusted based on experience to guarantee the reliable simulation results. In this paper, φ is set to be 10^{-4} m, which is equal to the maximum mesh size. χ is initially set to be 2 m·s/kg based on the default value. For different numerical simulation runs, both parameters φ and χ are adjusted accordingly.

4. Results

4.1 Spatial distribution of $scCO_2$ saturation, pore pressure and flow rate

In the numerical experiment of $scCO_2$ displacement at the pore scale, the CO_2 injected into water-wet porous media at a rate of 0.01 m/s displaces the saturated pore water or connate water and the $scCO_2$ moves forward along different flow channels (Ch) with time (Fig. 4). The $scCO_2$ firstly flows into the relatively large pores, while the relatively narrow throat restricts the flow of $scCO_2$. The viscous fingering effect of $scCO_2$ becomes much more obvious with time due to the heterogeneity in porous media (Fanchi, 2018). Ch1 is the most preferential flow channel for $scCO_2$ movement, followed by Ch2, Ch3 and Ch4.

Microscopic flow paths of $scCO_2$ changes with time,

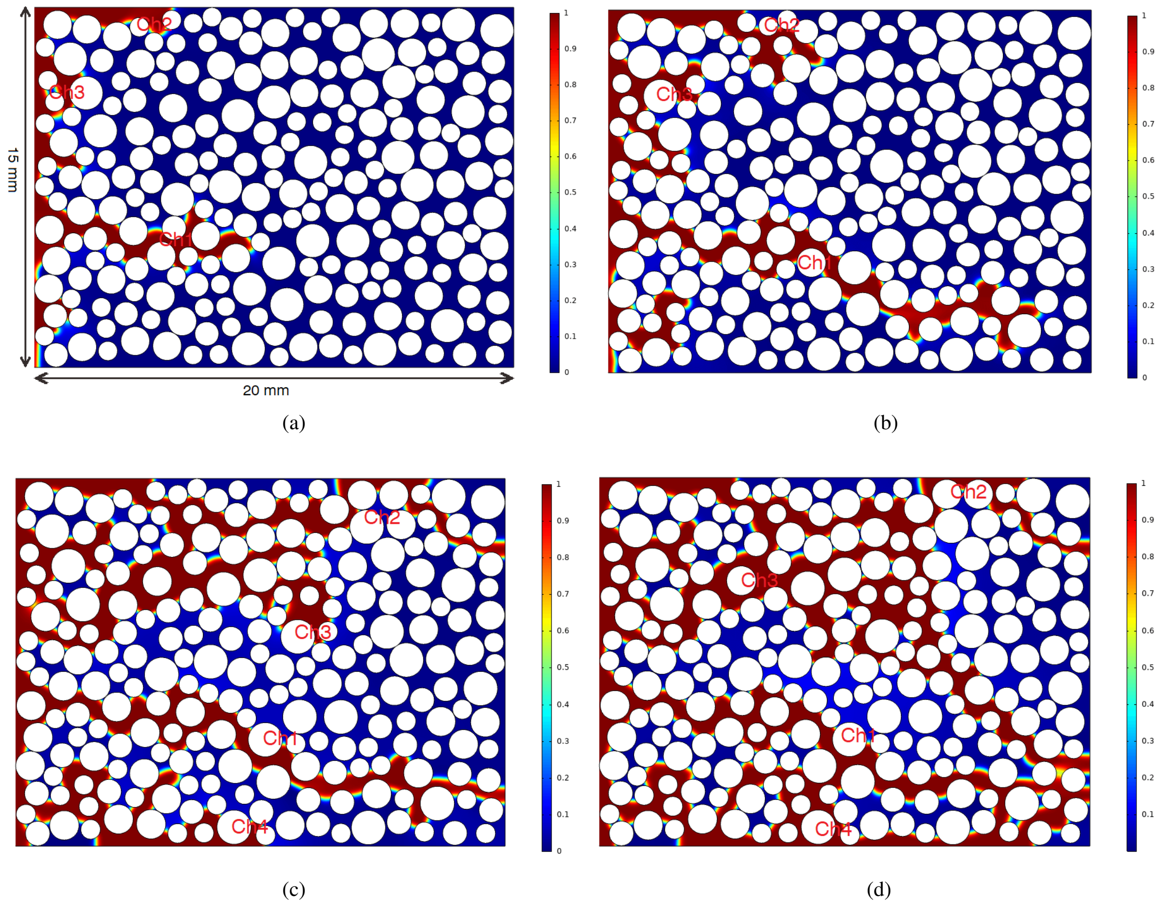

Fig. 4. The spatial distribution of $scCO_2$ in flow channels in porous media after different time of injection (a) 0.1 s; (b) 0.2 s; (c) 0.5 s; (d) 1.0 s (white spherical beads represent the grain particles of the sandstone reservoir, blue color represents water and red color represents the $scCO_2$).

allowing some $scCO_2$ to be trapped in porous media. The $scCO_2$ preferential flow paths correspond to high flow rates and high pore pressures occupied by $scCO_2$, see Fig. 5. The pore pressure distribution profile can be used to predict the movement of CO_2 front in the rock matrix. A preferential CO_2 migration path is bounded by the grains marked in the $scCO_2$ flow rate distribution of Fig. 6.

4.2 Variation of pore pressure with time in the preferential flow path

The spatial distribution of pore pressure at 0.1 s and 0.5 s after CO_2 injection from the left inlet can be seen in Figs. 5(b) and 5(d). The variation of pore pressure for three selected sampling points along one of the main flow path is shown in the Fig. 7. It shows that the pore pressure decreases sharply after CO_2 injection starts (< 0.01 s) for points a and b that are close to the inlet in Fig. 7. The connate water is displaced by the injected $scCO_2$ but the pressure of injected CO_2 is smaller than that of the water, thus the pore pressure decreases during the $scCO_2$ displacing the connate water process. The pore pressure close to the inlet tends to be a constant with continuous $scCO_2$ injection (see points a and b), indicating that the $scCO_2$ flow becomes a steady state. The pore pressure at the point c close to the outlet is not affected, demonstrating that no $scCO_2$ flows through the point c during the monitoring period.

The pore pressure along a whole selected preferential flow path at three different time (i.e., 0.01 s, 0.1 s, 1.0 s) is shown in Fig. 8. The maximum pore pressure difference between the two ends (i.e., inlet and outlet) is 800 Pa, which occurs after 0.1 s of CO_2 displacement process. It implies that the preferential flow path becomes unchanged with time and the pressure difference between the inlet and outlet of this flow path at 1.0 s is 350 Pa, which is 370 Pa lower than that of the value at 0.01 s.

5. Discussion

To study the impact of configuration of pores and fractures on $scCO_2$ flow paths and characteristics at the pore scale, different case studies are carried out considering impacts of various parameters including contact angle, wettability, interfacial tension of porous media, model geometry (either homogeneous or heterogeneous) and injection rates.

5.1 Effect of wettability

Quartz-rich sandstone is generally water-wet, but it may

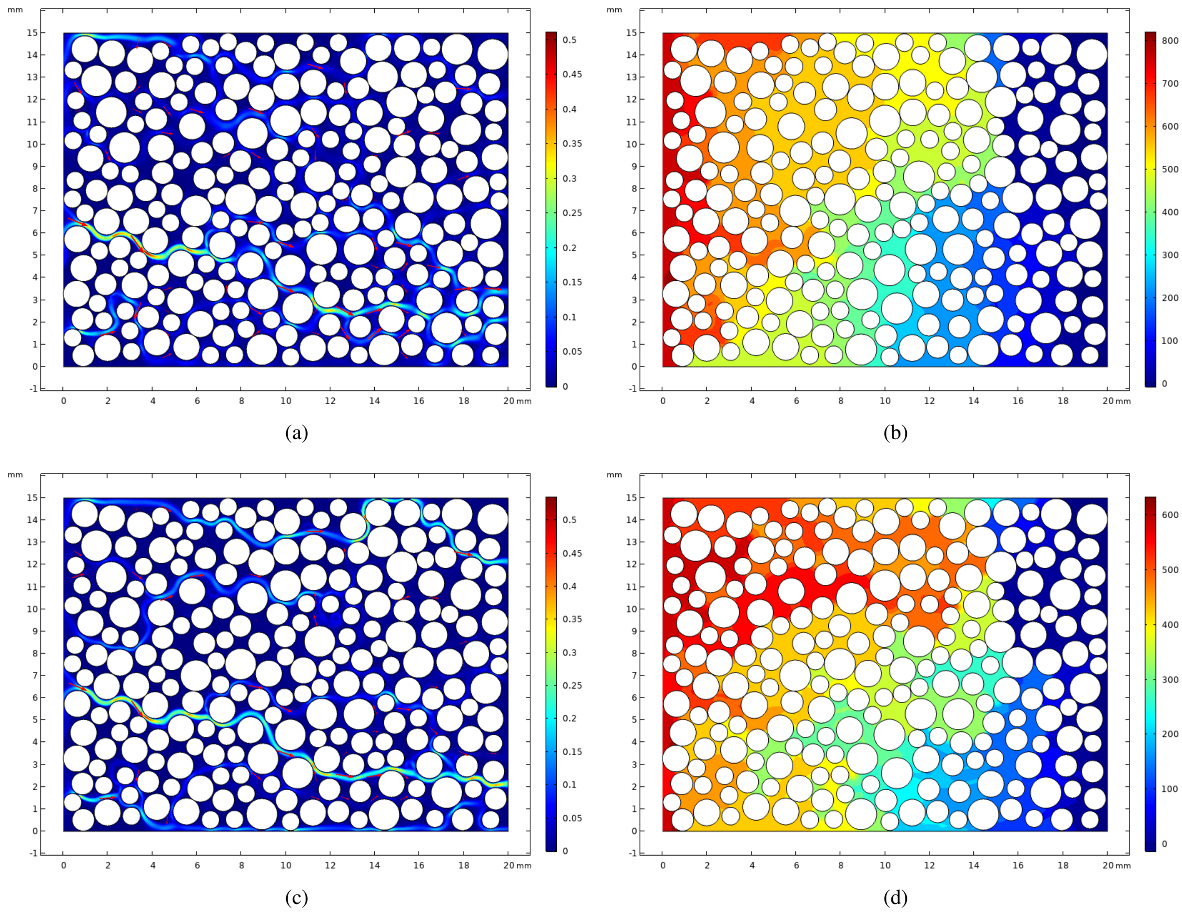

Fig. 5. (a) and (c) distribution of $scCO_2$ flow rates (m/s), (b) and (d) pore pressure (Pa) in the base case, after 0.1 s of $scCO_2$ injection in (a) and (b), 0.5 s of $scCO_2$ injection in (c) and (d).

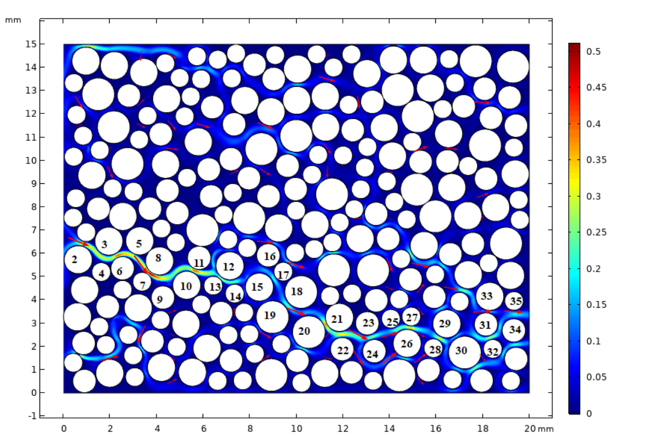

Fig. 6. The $scCO_2$ flow rate (unit: m/s) in porous media after 0.1 s of $scCO_2$ displacing in porous media with the injection rate of 10 mm/s at the inlet, representing the enlarged view of Fig. 5(a).

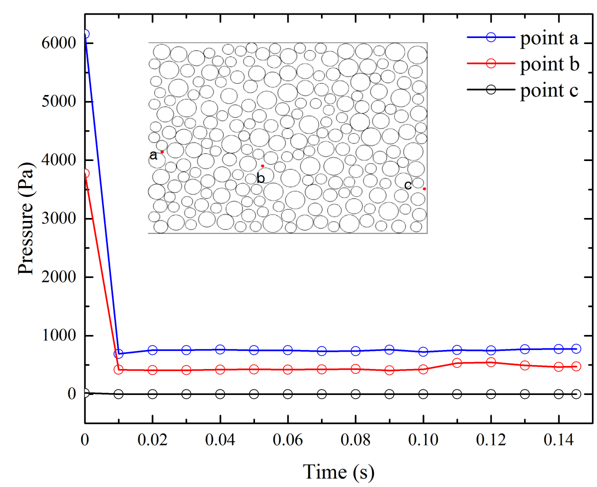

Fig. 7. The pore pressure changes at the monitoring points during the $scCO_2$ displacing process in porous media with the contact angle of 60° and the injection rate of 10 mm/s at the inlet.

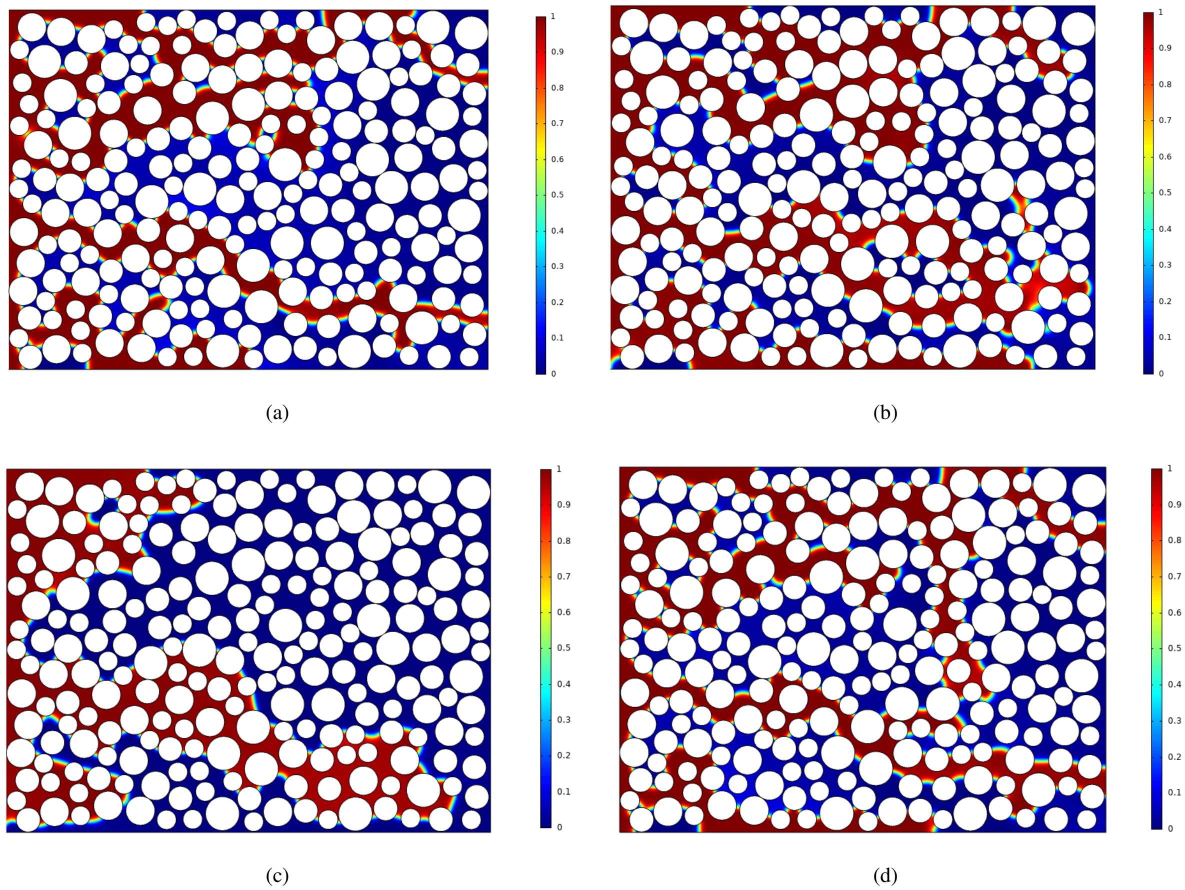

Fig. 9. Spatial distribution of $scCO_2$ in porous media after 0.5 s of CO_2 injection under different wettability with contact angles of (a) 60°; (b) 90°; and (c) 120°; and d) mixed wettability with the contact angles of 60° and 90°.

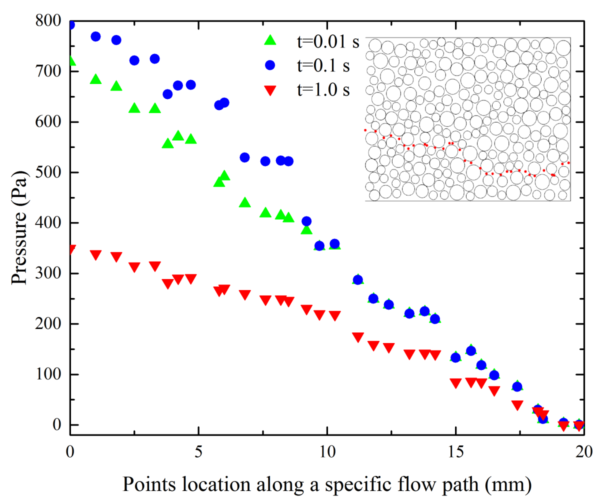

Fig. 8. The pore pressure changes along a selected main $scCO_2$ migration path at three different time in porous media with the contact angle of 60° and the injection rate of 10 mm/s at the inlet.

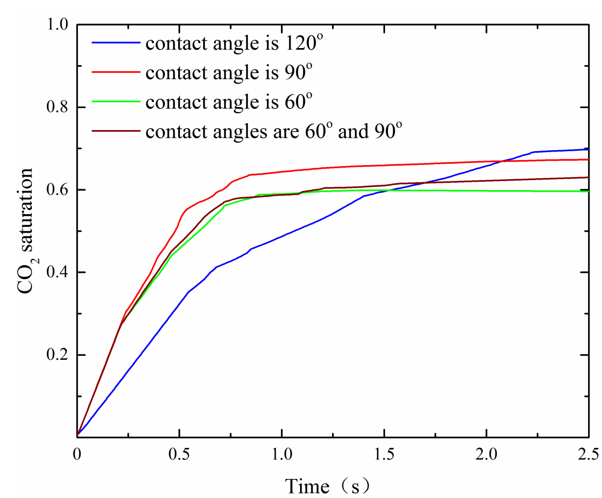

Fig. 10. The variation of CO_2 saturation in porous media with three different contact angles with the continuous injection of CO_2 at the inlet.

become mixed-wet (Krevor et al., 2012) or CO_2-wet (Iglauer et al., 2012) with the increase of clay contents. Thus, three cases including the water-wet with the contact angle of 60°, intermediate-wet with the contact angle of 90°, CO_2-wet with the contact angle of 120° and the mix-wet with the contact angle of 60° and 90° are considered in the simulation runs. It shows that the wettability of porous media dominates the migration paths of the $scCO_2$ but the main preferential flow paths are very similar between these four cases (Fig. 9). When the rock matrix is more water-wet, i.e., capillary forces are regarded as resistance and it is much difficult for $scCO_2$

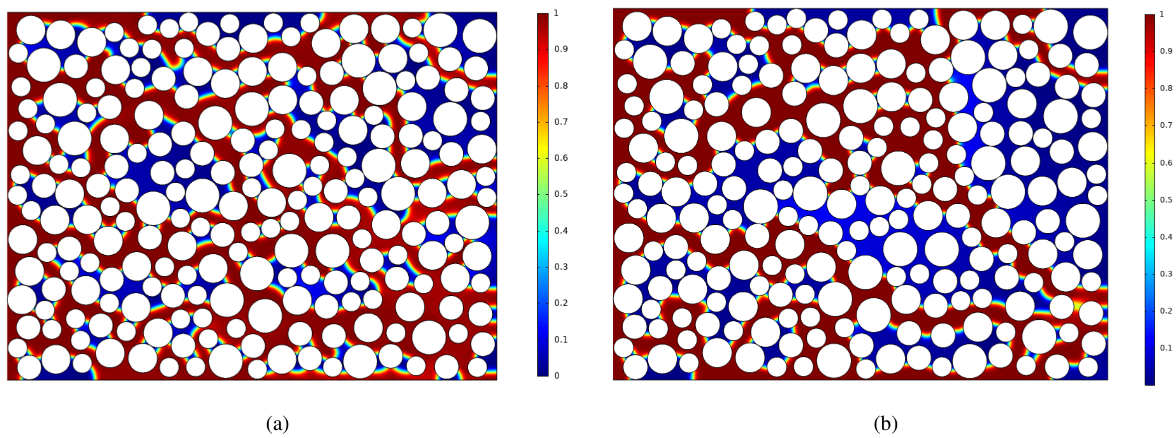

Fig. 11. Spatial distribution of $scCO_2$ saturation in porous media at $T = 1.0$ s after CO_2 injection under (a) the low (5 mN/m) and (b) high (27 mN/m) interfacial tension conditions.

migration. During the drainage process of $scCO_2$, water is gradually expelled and detached from the grains and the $scCO_2$ gradually migrates towards the outlet. The CO_2 saturation in porous media changes with the continuous injection of CO_2. The CO_2-wet porous media takes a much higher constant CO_2 saturation after 2.0 s of CO_2 displacement process, followed by the intermediate-wet with the contact angle of 90° and the mixed-wet condition, while water-wet porous media owns the lowest constant CO_2 saturation (see Fig. 10).

5.2 Effect of interfacial tension between two fluids

Under the same conditions of temperature and pressure, the interfacial tension of porous media can be changed due to variations in the concentration of $scCO_2$, salinity of the $scCO_2$-water system, etc (Xing et al., 2013). A low interfacial tension in the reservoir will much easily allow the supercritical CO_2 to penetrate through porous media in the middle parts of the pores or pore throats (Fig. 11(a)). However, when the interfacial tension is much higher in the $scCO_2$-water-rock system, the $scCO_2$ occupies less pore spaces and less migration paths (Fig. 11(b)). The changes of CO_2 saturation in porous media with time can be seen in Fig. 12. It shows that the larger interfacial tension results in much lower CO_2 saturation because of the much higher capillary pressure that hinders the CO_2 movement in water-wet porous media.

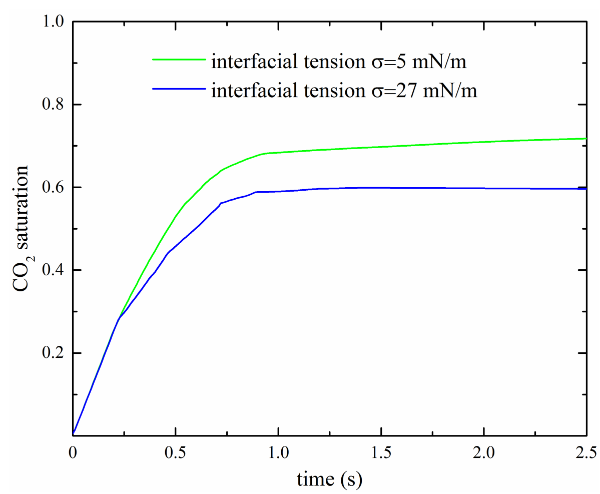

Fig. 12. Variation of the CO_2 saturation in porous media affected by different interfacial tension.

5.3 Effect of injection rates

The preferential flow behavior is obvious during the $scCO_2$ displacement process. Under much higher $scCO_2$ injection rates at the inlet, the $scCO_2$ filtration rates at the pore scale are much higher and the preferential flow is much more obvious under the constant injection volume (Fig. 13). The viscous fingering of $scCO_2$ becomes much obvious under high injection rates as viscous forces also become more significant (Lv et al., 2017). The CO_2 saturation with time is positive related with the CO_2 injection rates at the inlet (Fig. 14). The earlier constant CO_2 saturation reaches with a much higher CO_2 injection rate. With time, some injected CO_2 flows out of the outlet boundary. The much higher CO_2 injection rate will lead to a jump in the pore pressure (Fig. 15), implying the complexity of migration paths.

5.4 Effect of fracture configuration

To study the impacts of micro-cracks on the $scCO_2$ flow path, three types of fracture geometry are considered: 1) single fracture; 2) combination of main fracture and secondary fractures with different angles (Y-type and T-type); 3) combination of main fracture and discrete micro-fractures. The simplified circular grains are generated in the Matlab software, and small-size particles are manually deleted to form the main fracture in the AUTOCAD. The secondary and discrete micro-fractures can cut through the particles. The 2D geometry of fractured porous media generated by AUTOCAD is input in the Comsol Multiphysics simulator and the dimension of the 2D geometrical model is 20 mm in length and 15 mm in width. All the pores and fractures are discreted using the triangular

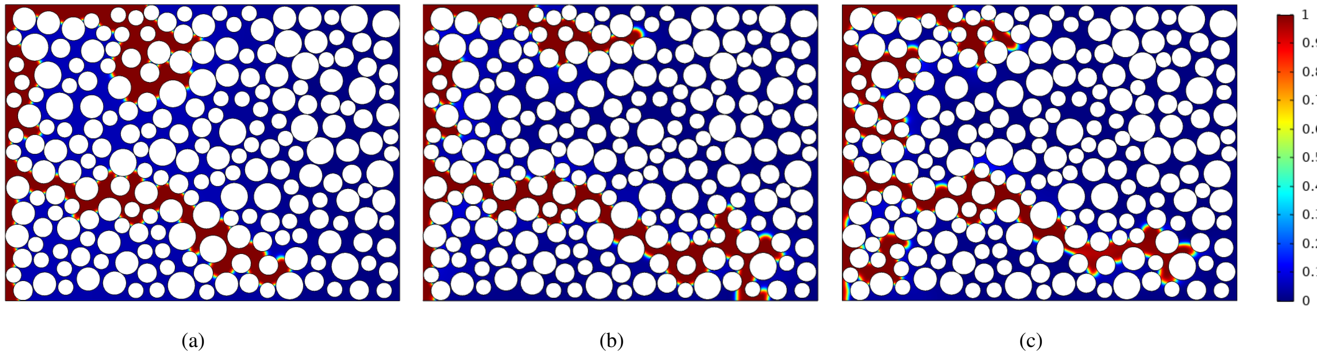

Fig. 13. The $scCO_2$ saturation in porous media after a constant volume (30 mm^3) of CO_2 injection under different injection rates a) 1 mm/s; b) 5 mm/s; c) 10 mm/s.

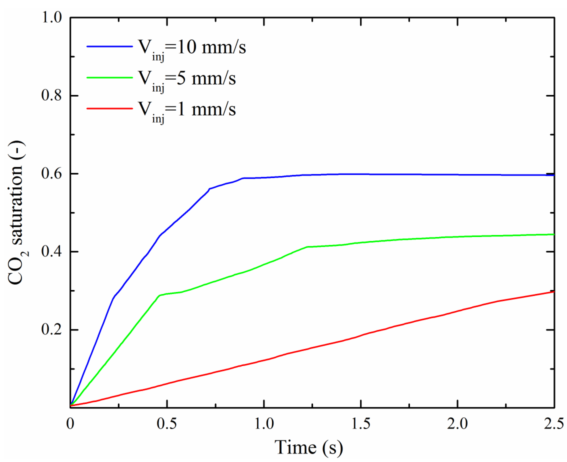

Fig. 14. The $scCO_2$ saturation with time after a constant volume (30 mm^3) of CO_2 injection under three different injection rates.

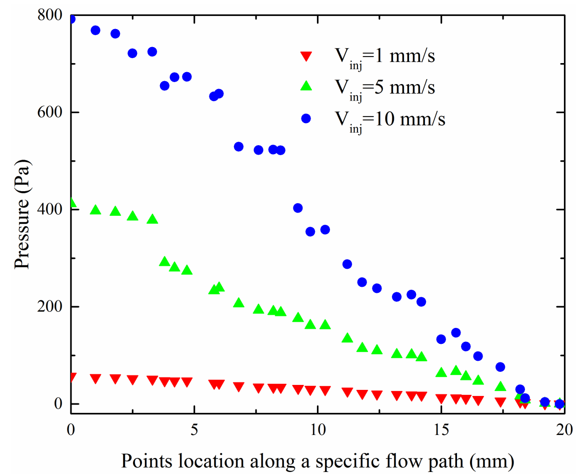

Fig. 15. Variation of pore pressure along the specific preferential flow path after 0.1 s CO_2 injection at the inlet under three different injection rates.

meshes in the 2D geometry, see similar processes shown in the Section 3.1.

Under the CO_2 injection rate of 10 mm/s at the inlet, fractures with large apertures become the preferential flow paths for the injected CO_2 (Fig. 16), while the small discrete fractures are not filled with the injected CO_2. When the CO_2 injection rate at the inlet increases, the small discrete fractures can weaken the $scCO_2$ flow in the main fracture by promoting the $scCO_2$ along the discrete fractures and increase the complexity of $scCO_2$ flow path and distribution in fractured porous media.

5.5 Effect of grain shapes

The variation of the grain shapes in porous media, which results in the reservoir heterogeneity (Sun and Bryant, 2014), will accordingly change the spatial distribution of $scCO_2$ migration paths as the intrinsic permeability of rock also changes (Lv et al., 2017). Based on microscopic observations of thin-sections, the sandstone is usually characterized with grains of irregular geometry, which greatly increases the tortuosity of fluid flow. Taking the thin-section of sandstone obtained from the Shiqianfeng formation in the Ordos Basin as an example (Fig. 17), a 2D geometry of porous media is constructed and used in the simulation.

The upper Permian Shiqianfeng formation (Fm. SQF), together with the middle Permian Shihezi formation (Fm. SHZ), lower Permian Shanxi formation (Fm. SX), and the lower Triassic Liujiagou formation (Fm. LJG), are selected as main storage aquifers for CO_2 storage in the first full-scale CO_2 sequestration project (i.e., Shenhua CO_2 capture and storage demonstration project) in the Ordos Basin, China (Liu et al., 2014b; Wei et al., 2014; Mkemai and Bin, 2020). At the end of 2015, about 0.302 million tons of CO_2 was injected underground since this project started in 2010. One of the main target CO_2 storage aquifers, i.e., the Fm. SQF, has a thickness of 291 m with the buried depth between 1699 and 1990 m and there are seven caprock-reservoir assemmblages characterized as purplish red feldspathic quartz sandstone mixed with silty mudstone (Jing et al., 2019). The mineralogy of Fm. SQF sandstone is mainly composed of quartz, oligoclase, K-feldspar and illite, and less proportion of kaolinite and calcite. The physical properties of sandstone aquifers used for CO_2 injection in the Ordos Basin based on measurement of 13 perforated intervals are listed in Table 2. It shows that the porosity of the sandstone obtained from the

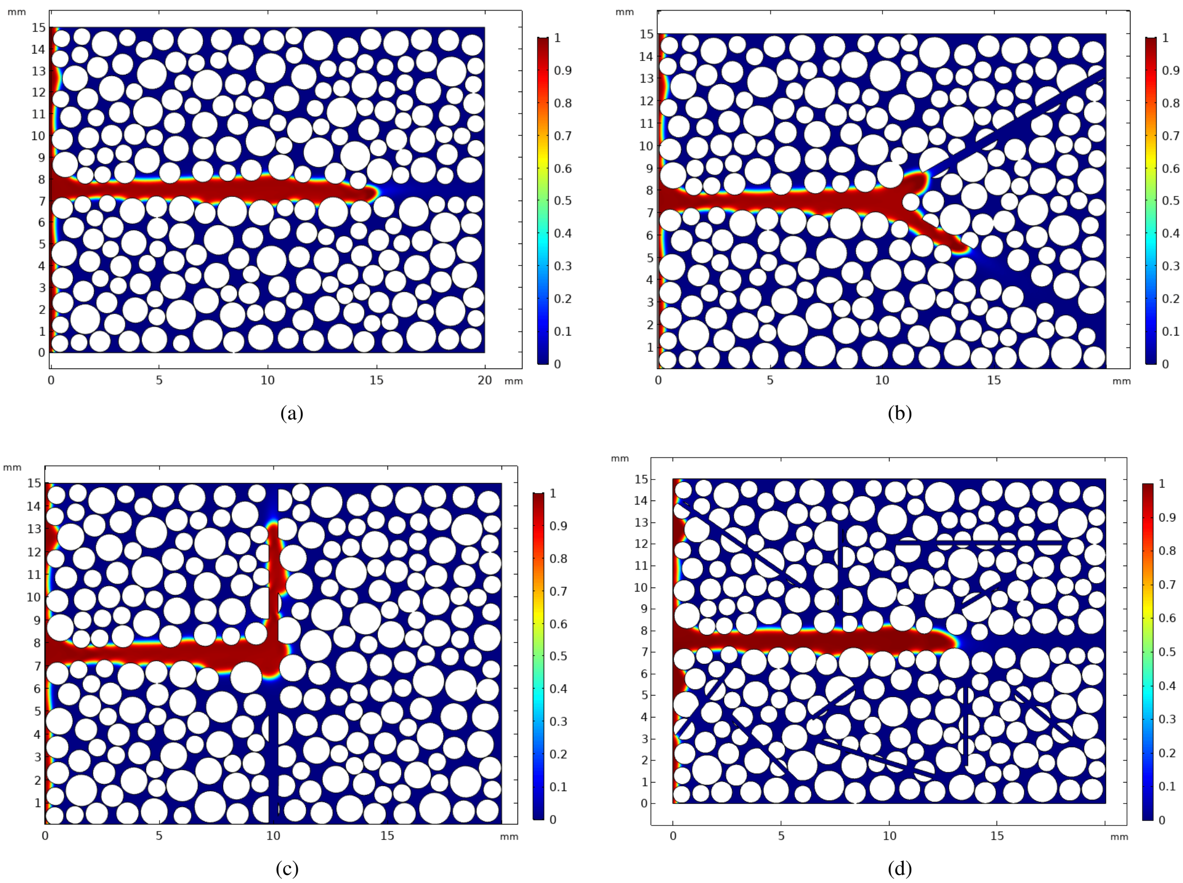

Fig. 16. The $scCO_2$ flow in fractured media at 0.1 s with a) a single fracture; b) a Y-type fracture; c) a T-type fracture; and d) many fractures at the injection rate of 10 mm/s. X and Y coordinates represent the position (mm).

Table 2. Physical properties of sandstone aquifers at perforated intervals for CO_2 injection in the Ordos Basin (Kuang et al., 2014).

Interval	Top depth (m)	Bottom depth (m)	Thickness (m)	Formations	Porosity (%)	Permeability (mD)
1	1,690.0	1,699.0	9.0	LJG	10.6	2.81
2	1,751.4	1,756.8	5.4	SQF	12.4	5.47
3	1,860.4	1,866.0	5.6	SQF	9.3	1.57
4	1,876.0	1,883.6	7.6	SQF	5.0	0.1
5	1,909.6	1,915.2	5.4	SQF	9.6	1.77
6	1,918.4	1,922.8	4.4	SQF	10.2	2.36
7	1,940.6	1,947.8	7.2	SQF	11.2	3.52
8	1,982.8	1,990.0	7.2	SQF	12.9	6.58
9	2,105.8	2,109.0	4.2	SHZ	12.6	5.9
10	2,167.0	2,175.6	8.6	SHZ	12.0	4.67
11	2,204.6	2,208.2	3.6	SHZ	12.2	5.03
12	2,241.2	2,262.0	20.8	SX	8.8	1.74
13	2,271.2	2,275.6	4.4	SX	11.3	4.48

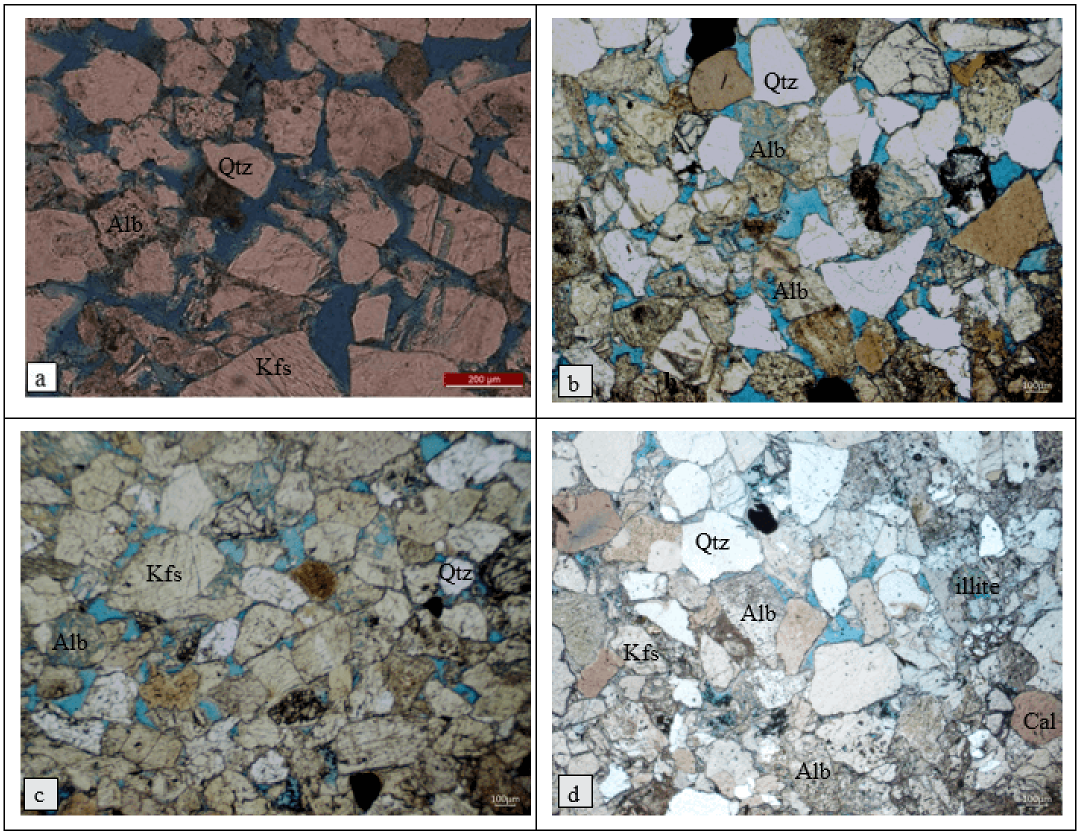

Fig. 17. The casting thin section analysis of Fm. SQF sandstone, showing pore space filled with blue-stained resin, quartz, calcite, feldspar, rock fragments.

Fm. SQF is in the range of 5.0%-12.9%, with an average value of 10.1%. The permeability of Fm. SQF is in the range of 0.1-6.58 mD, with the average value of 3.05 mD.

Based on the casting and scanning electron microscope data, it shows that the median grain size of rock debris obtained from Fm. SQF is 0.73 mm (Wan, 2012). The total surface porosity of SQF sandstone is 4.67% (Wu, 2011), which is the highest among the injection aquifers. The primary pores are mainly intergranular (2.55%), and the secondary pores are mainly intragranular, intergranular solution pores and micro-cracks (Zhou et al., 2017). Among them, the surface porosity induced by micro-cracks is 0.05%. The capillary pressure curve and relative permeability curve of sandstone obtained from the Fm. SQF have been measured by Diao (2017). The displacement pressure is 0.24 MPa and the average pore throat radius is 2.21 μm (Wu, 2011). The water chemistry of Shiqianfeng formation is characterized as Cl-Ca·Na, and the content of TDS is 31,212.34 mg/L (Diao, 2017).

The geometry of the 2D model is based on the image vectorization of Fig. 15(a), and the numerical model is set up considering the conditions of the Shiqianfeng formation in the Ordos Basin. It shows that at the beginning of the $scCO_2$ displacement, the water lock effect occurs obvious due to the $scCO_2$ migration along different paths (see Fig. 18(a)). With

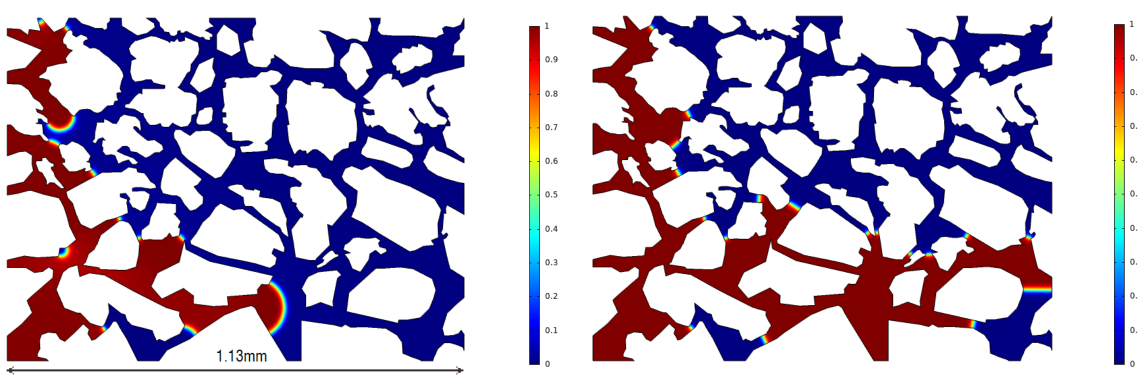

(a) (b)

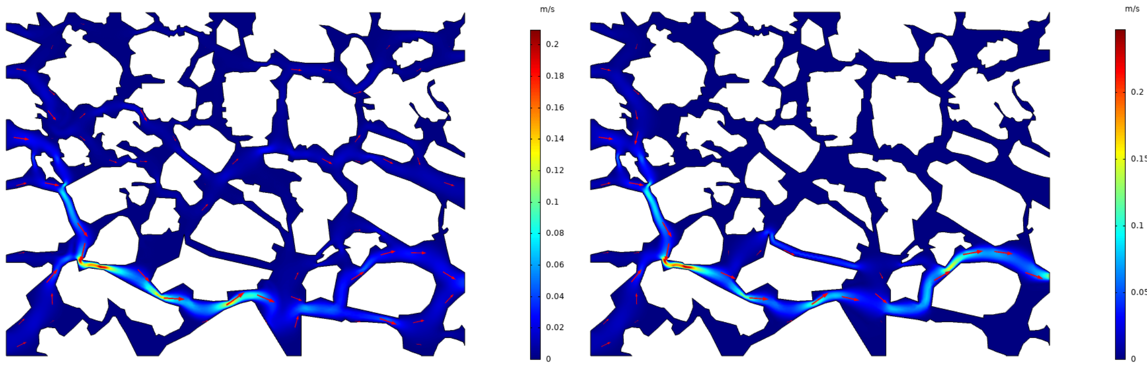

(c) (d)

Fig. 18. a) and b) the $scCO_2$ saturation distribution in porous media at 0.05 s and 0.5 s respectively (white color represents the rock skeleton); c) and d) the flow rates (m/s) of $scCO_2$ at 0.05 s and 0.5 s, respectively.

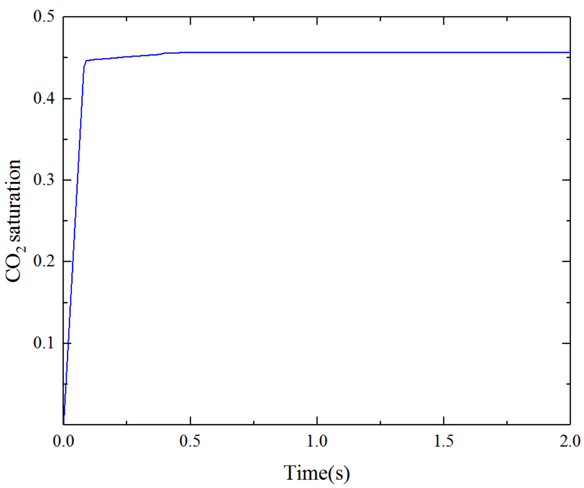

Fig. 19. The variation of CO_2 saturation with time in porous media extracted from Shiqianfeng formation.

time, the water lock effect still exists at local regions but it moves in porous media. Comparison of both the spatial distribution and flow rates of $scCO_2$ in porous media reveals a good correlation (see Figs. 18(b) and 18(d)). Preferential flow occurs adjacent to the grain or fracture walls with little or no flow in the interior of the grains, which is in accordance with the results by Chaudhary et al. (2013). As the reservoir heterogeneity in CO_2 storage region increases, the $scCO_2$ migration patters evolve from dispersed capillary channels to compact distributions as illustrated in Sun and Bryant (2014) and this paper. The CO_2 saturation increases sharply at the beginning of the injection period and it reaches to a constant value (i.e., 0.45) in porous media extracted from the Shiqianfeng formation (Fig. 19), demonstrating that the CO_2 flows along the relative constant paths with time.

6. Conclusions

Drainage and imbibition of connate water is a common phenomenon in fluid injection-production operations such as CO_2 geological sequestration, hydrocarbon production and geothermal exploitation. This paper works on the $scCO_2$ flow in the geological carbon dioxide sequestration which offers a powerful and efficient means for reducing CO_2 emissions to the atmosphere. Migration paths of $scCO_2$ are strongly influenced by the chemical interactions and the reservoir properties, thus controlling the injectivity and storage efficiency of $scCO_2$. Based on numerical experiments on $scCO_2$ displacement using the COMSOL Multiphysics simulator, some conclusions can be drawn as follows:

1) Models constituted of the random regular particles are useful in studying the $scCO_2$ displacement at the pore scale, but heterogeneity of porous or fractured media in the natural geological conditions makes it very difficult to track the $scCO_2$ migration at the regional scale.
2) Phase field method is powerful in tracking the boundaries between the $scCO_2$ and water, but the assignment of parameters is strongly empirical.
3) Heterogeneity of porous media caused by fractures with large apertures significantly dominates the migration paths of the $scCO_2$.
4) The migration paths of $scCO_2$ is not only affected by the CO_2 injection rates at the inlet, other factors including the interfacial tension, wettability or contact angle, etc., also affect the $scCO_2$ preferential flow paths at the local.
5) The pore pressure close to the inlet is strongly increased at the beginning of CO_2 injection, which tends to be a constant with continuous CO_2 injection and the steady flow of $scCO_2$ attains with time. But the preferential flow path changes with continuous injection of CO_2.
6) The CO_2 saturation in porous media is strongly affected by the contact angle of grains, and the CO_2-wet rock grains is easily for the CO_2 migration after a threshold time. High interfacial tension greatly hinders the CO_2 migration into the pores. The CO_2 injection rates at the inlet are proportional to the CO_2 saturation. For the Shiqianfeng formation sandstone, the maximum CO_2 saturation in porous media can attain a constant value of 0.45.

This paper considers $scCO_2$ displacing processes in porous/fractured media. Reactive chemical interactions and deformation of porous/fractured media, which also affect the $scCO_2$ drainage process at the pore scale, is still under investigation and will be released later.

Acknowledgement

We acknowledge the financial support of several projects including the National Natural Science Foundation of China (Grant Nos. 51809259, 51874202), the CAS Pioneer Hundred Talents Program in China, State Key Laboratory of Hydraulics and Mountain River Engineering affiliated to Sichuan University (No. SKHL1917), Key Laboratory of Deep Earth Science and Engineering (Sichuan University), Ministry of Education (No. DESE202002) and the Sichuan Youth Fund (No. 2017JQ0003).

Conflict of interest

The authors declare no competing interest.

References

Al-Futaisi, A., Patzek, T.W. Impact of wettability alteration on two-phase flow characteristics of sandstones: A quasi-static description. Water Resour. Res. 2003, 39(2): 1042.

Al-Shalabi, E.W., Ghosh, B. Effect of pore-scale heterogeneity and capillary-viscous fingering on commingled water-flood oil recovery in stratified porous media. J. Pet. Eng. 2016, 2016: 1708929.

Andrew, M., Bijeljic, B., Blunt, M. Reservoir condition pore-scale imaging of multiple fluid phases using X-ray microtomography. J. Vis. Exp. 2015, 96: e52440.

Antanovskii, L.K. A phase field model of capillarity. Phys. Fluids 1995, 7(4): 747-753.

Bachu, S. Screening and ranking sedimentary basins for sequestration of CO_2 in geological media in response to climate change. Environ. Geol. 2003, 44(3): 277-289.

Bai, F., He, X.M., Yang, X.F., et al. Three dimensional phase-field investigation of droplet formation in microfluidic flow focusing devices with experimental validation. Int. J. Multiphase Flow 2017, 93: 130-141.

Baldwin, B.A., Yamanashi, W.S. Detecting fluid movement and isolation in reservoir core with medical NMR imaging techniques. SPE Reservoir Eval. Eng. 1989, 4(2): 207-212.

Benson, S.M., Cole, D.R. CO_2 sequestration in deep sedimentary formations. Elements 2008, 4(5): 325-331.

Bogdanov, I., Kpahou, J., Kamp, A. Direct pore-scale modeling of two-phase flow through natural media. Paper Presented at Proceedings of the 2011 COMSOL Conference, Stuttgart, Germany, 26-28 October, 2011.

Cahn, J.W., Hilliard, J.E. Free energy of a nonuniform system. I. interfacial free energy. J. Chem. Phys. 1958, 28(2): 258-267.

Chalbaud, C., Robin, M., Egermann, P. Interfacial tension data and correlations of brine/CO_2 systems under reservoir conditions. Paper SPE 102918 Presented at SPE Annual Technical Conference and Exhibition, San Antonio, Texas, USA, 24-27 September, 2006.

Chaudhary, K., Cardenas, M.B., Wolfe, W.W., et al. Pore-scale trapping of supercritical CO_2 and the role of grain wettability and shape. Geophys. Res. Lett. 2013, 40: 3878-3882.

Chen, L.Q. Phase-field models for microstructure evolution. Annu. Rev. Mater. Res. 2002, 32(1): 113-140.

Combes, R., Robin, M., Blavier, G., et al. Visualization of imbibition in porous media by environmental scanning electron microscopy: Application to reservoir rocks. J. Pet. Sci. Eng. 1998, 20(3-4): 133-139.

Diao, Y.J. Study on the reservoir characterization and CO_2 migration underground in the Shenhua CCS demonstration project site. China University of Mining & Technology, Beijing, 2017.

Fanchi, J.R. Principles of Applied Reservoir Simulation-4th Edition. Gulf Professional Publishing, Oxford, United Kingdom, 2018.

Ginzburg, V.L., Landau, L.D. Towards the theory of super-conductivity. J. Exp. Theor. Phys. 1950, 20: 1064-1082.

Herring, A.L., Sheppard, A., Andersson, L., et al. Impact of wettability alteration on 3D nonwetting phase trapping and transport. Int. J. Greenhouse Gas Control 2016, 46: 175-186.

Holtz, M.H. Residual gas saturation to aquifer influx: A calculation method for 3-D computer reservoir model construction. Paper SPE 75502 Presented at SPE Gas Technologies Symposium, Calgary, Alberta, Canada, 30 April-2 May, 2002.

Holtzman, R. Effects of pore-scale disorder on fluid displacement in partially-wettable porous media. Sci. Rep. 2016, 6(1): 36221.

Holtzman, R., Segre, E. Wettability stabilizes fluid invasion into porous media via nonlocal, cooperative pore filling. Phys. Rev. Lett. 2015, 115(16): 164501.

Hu, R., Wan, J.M., Kim, Y., et al. Wettability impact on supercritical CO_2 capillary trapping: Pore-scale visualization and quantification. Water Resour. Res. 2017, 53(8): 6377-6394.

IEA. Caprock systems for CO_2 geological storage, 2011.

Iglauer, S., Ferno, M.A., Shearing, P., et al. Comparison of residual oil cluster size distribution, morphology and saturation in oil-wet and water-wet sandstone. J. Colloid Interface Sci. 2012, 375(1): 187-192.

Jacqmin, D. Calculation of two-phase Navier–Stokes flows using phase-field modeling. J. Comput. Phys. 1999, 155(1): 96-127.

Jamaloei, B.Y., Asghari, K., Kharrat, R., et al. Pore-scale two-phase filtration in imbibition process through porous media at high-and low-interfacial tension flow conditions. J. Pet. Sci. Eng. 2010, 72(3-4): 251-269.

Jing, J., Yang, Y.L., Tang, Z.H. Effects of formation dip angle and salinity on the safety of CO_2 geological storage-A case study of Shiqianfeng strata with low porosity and low permeability in the Ordos Basin, China. J. Clean. Prod. 2019, 226: 874-891.

Joshi, M.A. Class of stochastic models for porous media. University of Kansas, Lawrence Kansas, 1974.

Kareem, R. Towards a Nanoscopic understanding of oil-sandstone wettability-implications for enhanced oil recovery. Paper Presented at 18th European Symposium on Improved Oil Recovery, Dresden, Germany, 14-16 April, 2015.

Kizaki, A., Tanaka, H., Ohashi, K., et al. Hydraulic fracturing in Inada granite and Ogino tuff with supercritical carbon dioxide. Paper Presented at ISRM Regional Symposium-7th Asian Rock Mechanics Symposium, Seoul, Korea, 15-19 October, 2012.

Kobus, H., de Haar, U. Perspektiven der Wasserforschung, DFG, 1995.

Krevor, S.C.M., Pini, R., Zuo, L., et al. Relative permeability and trapping of CO_2 and water in sandstone rocks at reservoir conditions. Water Resour. Res. 2012, 48(2): W02532.

Kuang, D.Q., Li, Q., Wang, Y.S., et al. Numerical simulation of distribution of migration of CO_2 in Shenhua carbon capture and storage demonstration project. Rock Soil Mech. 2014, 35(9): 2623-2634.

Kumar, A., Noh, M.H., Sepehrnoori, K., et al. Carbon dioxide capture for storage in deep geologic formations-results from the CO_2 capture project: Vol. 2-geologic storage of carbon dioxide with monitoring and verification. Elsevier, London, UK, 2005.

Lenormand, R., Zarcone, C. Role of roughness and edges during imbibition in square capillaries. Paper SPE 13264 Presented at 59th SPE Annual Technical Conference and Exhibition, Houston, TX, 16-19 September, 1984.

Liu, H.J., Hou, Z.M., Li, X.C., et al. A preliminary site selection system for a CO_2-AGES project and its application in China. Environ. Earth Sci. 2015, 73(11): 6855-6870.

Liu, H.J., Hou, Z.M., Were, P., et al. Simulation of CO_2 plume movement in multilayered saline formations through multilayer injection technology in the Ordos Basin, China. Environ. Earth Sci. 2014a, 71(10): 4447-4462.

Liu, H.J., Hou, Z.M., Were, P., et al. Modelling CO_2-brine-rock interactions in upper Paleozoic formations of Ordos Basin used for CO_2 sequestration. Environ. Earth Sci. 2014b, 73(5): 2205-2222.

Liu, H.J., Li, Q., Were, P., et al. Worldwide status of CCUS technologies and their development and challenges in China. Geofluids 2017, 2017: 6126505.

Lv, P.F., Liu, Y., Chen, J.L., et al. Pore-scale investigation of effects of heterogeneity on CO_2 geological storage using stratified sand packs. Greenhouse Gases: Sci. Technol. 2017, 7(6): 972-987.

Mattax, C.C., Kyte, J.R. Ever see a water flood? Oil Gas J. 1961, 59: 115-128.

Metz, B., Davidson, O., de Coninck, H.C., et al. IPCC special report on carbon dioxide capture and storage. Cambridge University Press, Cambridge and New York, 2005.

Miao, X., Wang, Y., Zhang, L., et al. Improved Vinegar & Wellington calibration for estimation of fluid saturation and porosity from CT images for a core flooding test under geologic carbon storage conditions. Micron 2019, 124: 102703.

Minto, J.M. Towards a rational design of gravel media water treatment filters: MRI investigation of the spatial heterogeneity in pollutant particle accumulation. University of Glasgow, Glasgow, 2014.

Mkemai, R.M., Gong, B. A modeling and numerical simulation study of enhanced CO_2 sequestration into deep saline formation: A strategy towards climate change mitigation. Mitig. Adapt. Strateg. Glob. Chang. 2020, 25: 901-927.

Obdam, A., van der Meer, L.G.H., May, F., et al. Effective CO_2 storage capacity in aquifers, gas fields, oil fields and coal fields. Paper Presented at Proceedings of the 6th International Conference on Greenhouse Gas Control Technologies, Kyoto, Japan, 1-4 October, 2002.

Osher, S., Sethian, J.A. Fronts propagating with curvature dependent speed: Algorithms based on Hamilton-Jacobi formulations. J. Comput. Phys. 1988, 79(1): 12-49.

Parry, M., Canziani, O., Palutikof, J., et al. Climate change: Impacts, adaptation and vulnerability. IPCC, 2007.

Perrin, J.C., Benson, S.M. An experimental study on the influence of sub-core scale heterogeneities on CO_2 distribution in reservoir rocks. Transp. Porous Media 2010, 82(1): 93-109.

Prather, C.A. NMR studies of supercritical CO_2 in carbon sequestration and immiscible two phase flow in porous media. Montana State University, Bozeman, 2015.

Raeini, A.Q., Blunt, M.J., Bijeljic, B. Modelling two-phase flow in porous media at the pore scale using the volume-of-fluid method. J. Comput. Phys. 2012, 231(17): 5653-5668.

Rokhforouz, M.R., Akhlaghi Amiri, H.A. Phase-field simulation of counter-current spontaneous imbibition in a fractured heterogeneous porous medium. Phys. Fluids 2017, 29(6): 062104.

Shakibaeinia, A., Jin, Y.C. Mesh-free lagrangian modeling of mutiphase flow. Paper Presented at Proceedings of 20th Annual Conference of the CFD Society of Canada, Canmore, Alberta, 9-11 May, 2012.

Singh, H. Impact of four different CO_2 injection schemes on extent of reservoir pressure and saturation. Adv. Geo-Energy Res. 2018, 2(3): 305-318.

Song, Y.C., Jiang, L.L., Liu, Y., et al. An experimental study on CO_2/water displacement in porous media using high-resolution Magnetic Resonance Imaging. Int. J. Greenhouse Gas Control 2012, 10: 501-509.

Suekane, K., Furukawa, N., Tsushima, S., et al. Application of MRI in the measurement of two phase flow of supercritical CO_2 and water in porous rocks. J. Porous Media 2009, 2(12): 143-154.

Suekane, T., Izumi, T., Okada, K. Capillary trapping of supercritical CO_2 in porous media at the pore scale. Comput. Methods Multiphase Flow VI, WIT Trans. Eng. Sci. 2011, 70: 311-320.

Sun, Y.H., Bryant, S.L. Influence of grain size distribution and varying heterogeneity on local capillary trapping. Energy Procedia 2014, 63: 5607-5618.

Sun, Y.K., Li, Q., Fan, C.K. Laboratory core flooding experiments in reservoir sandstone under different sequestration pressures using multichannel fiber bragg grating sensor arrays. Int. J. Greenhouse Gas Control 2017, 60: 186-198.

Trojer, M., Szulczewski, M.L., Juanes, R. Stabilizing fluid-fluid displacements in porous media through wettability alteration. Phys. Rev. Appl. 2015, 3(5): 054008.

Turner, M.L., Knüfing, L., Arns, C.H., et al. Three-dimensional imaging of multiphase flow in porous media. Phys. A 2004, 339(1-2): 166-172.

Van der Waals, J.D. The thermodynamic theory of capillarity under the hypothesis of a continuous variation of density. J. Stat. Phys. 1979, 20(2): 200-244.

Wan, Y.Y. Migration and transformation of CO_2 in CO_2 geological sequestration process of Shiqianfeng saline aquifers in Ordos Basin. Jilin University, Changchun, 2012.

Wang, T., Song, Y., Zhao, Y., et al. Measurement of immiscible CO_2 flooding processes and permeability reduction due to asphaltene precipitation by X-ray CT imaging. Energy Proced 2013, 37: 6920-6927.

Wei, N., Gill, M., Crandall, D., et al. CO_2 flooding properties of Liujiagou sandstone: influence of sub-core scale structure heterogeneity. Greenhouse Gases: Sci. Technol. 2014, 4(3): 400-418.

Wu, W.H. Research on the characteristics and diagenesis of sandstone in the Upper Paleozoic reservoir in Ordos Basin. Chengdu University of Technology, Chengdu, 2011.

Xing, W.L., Song, Y.C., Zhang, Y., et al. Research progress of the interfacial tension in supercritical CO_2-water/oil system. Energy Procedia 2013, 37: 6928-6935.

Xu, L., Li, Q., Zhang, X.Y. Migration and storage characteristics of supercritical CO_2 in anisotropic sandstones with clay interlayers based on X-CT experiments. J. Hydrol. 2020, 580: 124239.

Xu, R.N., Luo, S., Jiang, P.X. Pore scale numerical simulation of supercritical CO_2 injecting into porous media containing water. Energy Procedia 2011, 4: 4418-4424.

Yan, W.C., Sun, J.M. Analysis of research present situation of microscopic remaining oil. Progress in Geophysics 2016, 31(5): 2198-2211. (in Chinese)

Yeong, C.L.Y., Torquato, S. Reconstructing random media: Three-dimensional media from two-dimensional cuts. Phys. Rev. E 1998, 58(1): 224-233.

Youssef, S., Bauer, D., Bekri, S., et al. 3D in-situ fluid distribution imaging at the pore scale as a new tool for multiphase flow studies. Paper SPE 135194 Presented at SPE Annual Technical Conference and Exhibition, Florence, Italy, 19-22 September, 2010.

Yu, M.H., Song, Y.C., Jiang, L.L., et al. CO_2/water displacement in porous medium under pressure and temperature conditions for geological storage. Energy Procedia 2014, 61: 282-285.

Yue, P.T., Feng, J.J., Liu, C., et al. A diffuse-interface method for simulating two-phase flows of complex fluids. J. Fluid Mech. 2004, 515: 293-317.

Yue, P.T., Zhou, C.F., Feng, J.J., et al. Phase-field simulations of interfacial dynamics in viscoelastic fluids using finite elements with adaptive meshing. J. Comput. Phys. 2006, 219(1): 47-67.

Zhang, Y., Nishizawa, O., Kiyama, T., et al. Flow behavior of supercritical CO_2 and brine in Berea sandstone during drainage and imbibition revealed by medical X-ray CT images. Geophys. J. Int. 2014, 197(3): 1789-1807.

Zhou, J., Hu, N., Xian, X., et al. Supercritical CO_2 fracking for enhanced shale gas recovery and CO_2 sequestration: Results, status and future challenges. Adv. Geo-Energy Res. 2019, 3(2): 207-224.

Zhou, X.Q., Zhang, Z.S., Zhang, C., et al. A new lithologic classification method for tight sandstone reservoirs based on rock components and logging response characteristics. J. Geophys. Eng. 2017, 14(6): 1599-1607.

Zhu, Q.L., Zhou, Q.L., Li, X.C. Numerical simulation of displacement characteristics of CO_2 injected in pore-scale porous media. J. Rock Mech. Geotech. Eng. 2016, 8(1): 87-92.